Extreme compression of LES flow data

Omar A. Mures[1][0000−0002−6042−3588],
Miguel Cid Montoya[2][0000−0002−3647−6022], and
Sumit Verma[2][0000−0003−3656−5022]

[1] XLab, Dept. of Civil Eng., University of A Coruña, Spain omar.alvarez@udc.es
[2] ASTRO Lab, Glenn Dept. of Civil Eng., Clemson University, USA
{mcidmon,sumitv}@clemson.edu

The increasing reliability of Computational Fluid Dynamics (CFD) simulations has established them as essential tools for aerodynamic analysis and wind-resistant design in many engineering fields. Simultaneous advancements in exascale computing have facilitated the development of large-scale models producing massive datasets. While offering significant advantages, storing and processing these massive datasets, particularly those produced by 3D Large Eddy Simulations (LES), poses a marked challenge for conventional methods. With their ability to directly solve large-scale turbulent structures and model small-scale turbulence, LES simulations provide a highly accurate but storage-intensive representation of aerodynamic phenomena. This work presents a novel compression method specifically designed to address this challenge. The proposed approach focuses on critical flow region compression by employing Implicit Neural Representations (INRs) and the Signed Distance Function (SDF), enabling accurate flow detail reproduction near surfaces of interest. Consequently, a new and efficient neural network architecture tailored for 3D and spatiotemporal compression is introduced. The developed framework delivers more efficient data storage, facilitating flow processing and flow feature visualization. The efficacy of this methodology is tested through a large-scale 3D LES simulation of a bridge deck resembling the Sunshine Skyway Bridge in Tampa, Florida, USA.

Keywords: compression · neural networks · CFD simulations.

1 Introduction

CFD simulations are integral to addressing many civil engineering challenges. The escalating complexity of contemporary problems, coupled with the enhanced availability of computational resources, has fueled a rapid increase in the scale of current simulations. Furthermore, this tendency has facilitated the adoption of engineering workflows that rely on iterative evaluations of large-scale simulations, including uncertainty quantification, wind-resistant design, and optimization. The subsequent exascale computing trends make data storage and analysis the major bottlenecks to be addressed in the near future [3]. Examples of large-scale CFD simulations in several wind and civil engineering fields include tall buildings [19], long-span bridges [25], wind environment analysis [11], and many others [4]. In some recent applications, simulations use meshes with more than

100 M cells [9] and very small time steps (e.g., $\Delta t = 0.00002$ s in [12]). The naive storage of flow fields generated by these demanding simulations inevitably results in the generation of massive flow field datasets.

Within bridge engineering, the development of wind-resistant design frameworks for bridge deck tailoring and optimization [5] necessitates aerodynamic analyses of multiple deck shape candidates. Although certain analyses, such as the extraction of bridge deck flutter derivatives via forced vibration simulations [17, 23, 30], can be performed using two-dimensional Unsteady Reynolds-Averaged Navier-Stokes (URANS) models, three-dimensional Large Eddy Simulation (LES) is indispensable for the accurate reproduction of complex fluid-structure interaction (FSI) problems, such as vortex-induced vibration (VIV) [2, 31], significantly elevating computational resource requirements. Moreover, the complex, nonlinear dependencies of FSI parameters on deck geometry, reduced velocity, and angle of attack require more advanced emulation strategies than classical interpolation of integrated, or "global," FSI metrics like flutter derivatives [6]. Advanced emulation techniques, particularly those based on deep learning, require the storage of detailed flow fields and force time series, which drastically exacerbates the data storage burden associated with modern CFD simulations. Addressing this challenge calls for transformative data management approaches that make storage feasible, enabling efficient training of emulators, and the development of robust emulation strategies.

Existing state-of-the-art compression techniques often inadequately leverage domain-specific information, thereby hindering the achievement of high compression ratios and precise flow field representations. Our objective is to achieve maximal storage reduction while preserving data fidelity, circumventing the inherent limitations of classical lossless compression algorithms such as bzip2 [26], the Lempel-Ziv-Markov chain algorithm (LZMA) [32], Prediction by Partial Matching (PPMd) [7], and OpenFOAM compression (Deflate [8]). These methods typically yield low compression ratios, due to lossless compression being fundamentally constrained by Shannon's entropy limit [27]. While approaches specifically tailored for scientific data, such as tensor-to-tensor compression [13], and established lossy techniques like MultiGrid Adaptive Reduction of Data (MGARD) [1], achieve higher compression ratios, between ∼5:1 and ∼60:1, these are often insufficient for the efficient storage of extensive simulation datasets on commodity hardware. Furthermore, these conventional compression methods typically lack integrated visualization and real-time analysis capabilities, necessitating computationally expensive decompression steps that hinder interactive workflows. Methodologies leveraging domain information and Implicit Neural Representations (INRs) [15, 16, 22] have demonstrated improved compression ratios, ranging from ∼40:1 and ∼100:1 when prioritizing low reproduction errors. Nevertheless, for applications demanding precise aerodynamic analysis, their reported performance generally trails that of our proposed methodology.

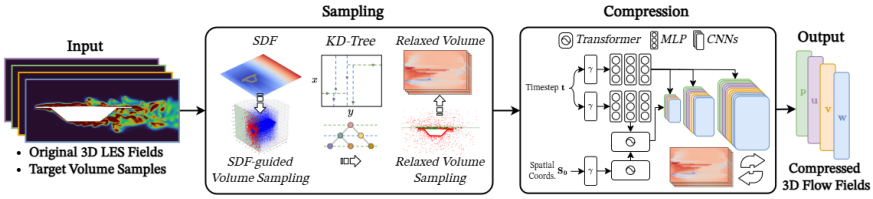

Fig. 1. Developed framework for LES flow field compression. The only necessary input is the simulation timestep value $\boldsymbol{t}$, that together with pre-computed $\boldsymbol{S}_0$ spatial coordinate values, will be used by the neural network to produce the corresponding $\boldsymbol{p}$, $\boldsymbol{u}$, $\boldsymbol{v}$, and $\boldsymbol{w}$. γ represents our positional encoding procedure. The architecture comprises two Multi-layer Perceptrons (MLPs), two transformers, and several convolutional decoders for flow field reconstruction.

2 Proposed framework for compression of flow data

Our framework for the compression of 3D LES simulations for analysis and visualization considers that data can be represented for each time step (t) in the form of an image volume $\psi_t \in \mathbb{R}^{d \times w \times h}$. Our goal is to reconstruct the volume series for all simulation time steps: ψ_t, $\forall t = 1, \ldots, T$. Being T the total number of time steps in the simulation. Since initially we do not have a spatially coherent storage data structure, but the unsorted data of each simulation cell center, a scheme for discretizing and spatially organizing the aforementioned information losing minimal fidelity is required.

2.1 Sampling

Conventional volume sampling methods (uniform or variable-density) generally fail to capture critical near-body flow details. We leverage a novel approach that employs the Signed Distance Function (SDF) [21] (see Fig. 1). By utilizing the SDF, our technique prioritizes sampling cell centers near bluff-body surfaces or important user-defined areas. The developed sampling method ensures high-fidelity reconstruction of critical flow regions, while regions of lower significance are subject to sparse sampling.

2.2 Compression

Inspired by INRs, such as [28], we propose an extension of the E-NeRV [14] architecture, specifically adapted to compress volumetric information. This novel model architecture is designed to further reduce the storage required by our volumetric representation of three-dimensional simulation data. The neural network will learn the mapping function $f_\theta : \mathbb{R} \rightarrow \mathbb{R}^{4 \times d \times h \times w}$ (see Fig. 1), with θ being the neural network's trainable parameters. We use the following positional encoding strategy to generate our temporal embeddings:

$$\gamma(\mathbf{t}) = \left[\sin(b^0 \pi \mathbf{t}), \cos(b^0 \pi \mathbf{t}), \ldots, \sin(b^{l-1} \pi \mathbf{t}), \cos(b^{l-1} \pi \mathbf{t})\right]^T \quad (1)$$

The hyperparameters b and l are optimized trough a dedicated tuning process. For spatial coordinates ($\boldsymbol{S}_0$) the same $\gamma(\cdot)$ encoding procedure is followed. Our architecture is designed to effectively disentangle and then fuse spatiotemporal representations, with temporal information injected at each stage of the decoder by a compact Multi-Layer Perceptron (MLP) [24]. For explicit feature fusion, a second MLP generates another set of temporal embeddings. Concurrently, a dedicated transformer module [29] produces spatial embeddings. These distinct temporal and spatial embeddings are subsequently fed into a small-scale fusion transformer, also based on the attention mechanism, which is responsible for integrating the spatio-temporal information. Finally, the features emerging from this fusion transformer are processed by a series of convolutional decoders to reconstruct the desired output flow field variables: pressure ($\boldsymbol{p}$) and the velocity components ($\boldsymbol{u}$, $\boldsymbol{v}$, $\boldsymbol{w}$).

3 Application case: 3D LES of a single-box bridge deck

A single-box deck similar to the deck cross-section of the Sunshine Skyway Bridge is used as a test case. The geometrical configuration of the cross-section is explained in detail in [30], where forced vibration simulations using 2D URANS of several deck shape modifications were studied. The current investigation studies the aerodynamics of the non-moving deck with aspect ratio $H/B = 0.1556$. Details of the computational modeling are provided below.

3.1 3D LES computational modeling

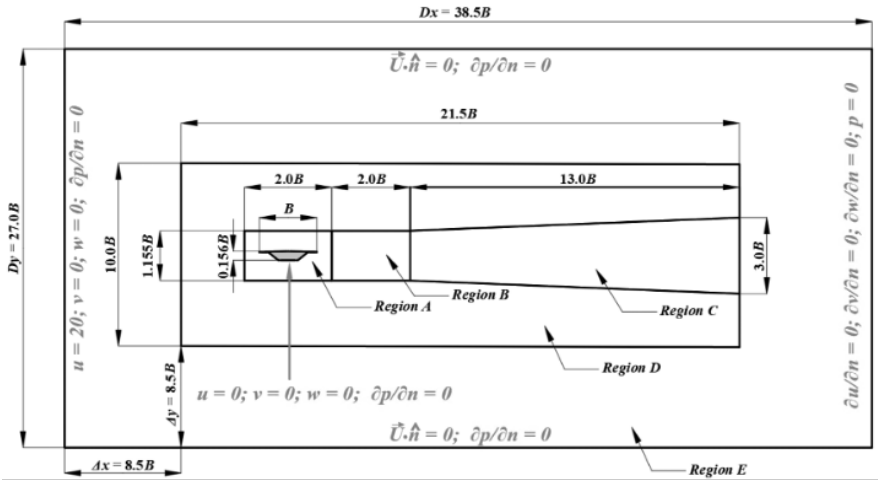

Fig. 2. Discretization of the computational domain with refinement regions.

The 3D computational domain is comprised of a cuboid of dimension $38.5B$ x $27B$ x B in the $x-$, $y-$ and the $z-$direction respectively. The dimension B is the top width of the bridge deck, which is equal to $B = 0.45$ m. The flow in the computational domain is modeled using the incompressible Navier-Stokes equation. The governing equation of the fluid flow around the static bridge deck is as follows, where the spatially filtered field variables are represented by a tilde ($\tilde{}$) over them:

$$\frac{\partial\left(\tilde{U_i}\right)}{\partial x_i} = 0 \tag{2a}$$

$$\rho\frac{\partial\tilde{U_i}}{\partial t} + \rho\frac{\partial\left(\tilde{U_i}\tilde{U_j}\right)}{\partial x_j} = -\frac{\partial\tilde{P}}{\partial x_i} + \frac{\partial}{\partial x_j}\left[\mu\left(\frac{\partial\tilde{U_i}}{\partial x_j} + \frac{\partial\tilde{U_j}}{\partial x_i}\right) - \rho\tau_{SGS}\right] \tag{2b}$$

where τ_{SGS} is the subgrid scale stress tensor, which is modeled using the WALE (Wall Adapting Local Eddy Viscosity) model [20]. The subgrid scale stress tensor is related to the mean strain-rate tensor by Eq. (3) and the mean strain-rate tensor is given by Eq. (4).

$$\tau_{SGS} = -2\nu_{SGS}\bar{S_{ij}} \tag{3}$$

$$\bar{S_{ij}} = \frac{1}{2}\left(\nabla\tilde{U} + \nabla\tilde{U}^T\right) \tag{4}$$

The sub-grid scale viscosity (ν_{SGS}) is computed using:

$$\nu_{SGS} = (C_W\Delta)^2\frac{(S^d_{ij}S^d_{ij})^{3/2}}{(\bar{S_{ij}}\bar{S_{ij}})^{5/2} + (S^d_{ij}S^d_{ij})^{5/4}} \tag{5}$$

In Eq. (5), C_W is the model coefficient, which is equal to $C_W = 0.325$ and Δ is the filter width (equal to the cube root of volume of the Control Volume (CV) cells) and S^d_{ij} is the filtered velocity gradient tensor given by:

$$S^d_{ij} = \frac{1}{2}\left(\frac{\partial\bar{u}_i}{\partial x_k}\frac{\partial\bar{u}_k}{\partial x_j} + \frac{\partial\bar{u}_j}{\partial x_k}\frac{\partial\bar{u}_k}{\partial x_i}\right) - \frac{1}{3}\delta_{ij}\left(\frac{\partial\bar{u}_k}{\partial x_l}\frac{\partial\bar{u}_l}{\partial x_k}\right) \tag{6}$$

For further numerical details, readers are directed to the original work of Nicoud and Ducros (1999) [20].

3.2 Spatial discretization of the computational domain

A 3D cuboidal domain is considered for flow modeling around the bridge deck and the cuboidal domain is divided into 5 regions, i.e., Region A, B, C, D, and E, with varying levels of refinement to capture the vortical flow structures formed in the vicinity of the bridge deck including the wake formed on the downstream side of the bridge deck with adequate resolution while still maintaining a low cell

count. The total number of CV cells in the domain is 7 790 700. The total length of the domain in the horizontal direction is $D_x = 38.5B$ and in the vertical direction is $D_y = 27.0B$ and along the spanwise direction is $D_z = B$, where B is the width of the deck. The dimensional details about the computational domain, along with the different refinement regions, comprising maximum and minimum cell sizes and growth rate are reported in Table 1 and Fig. 2.

The computational mesh is characterized by several key parameters. The height of the first cell layer within the boundary layer (BL) is $y_1/B = 6.67$ x 10^{-5}. This BL region consists of $N_{BL} = 10$ layers of hexahedral cells. In the span-wise direction, $N_z = 150$ cell layers are employed, and there are $N_H = 525$ cells around the deck perimeter. These specifications result in a total of 787 500 cells within BL, with a thickness of $y_{BL}/B = 0.022$. A detailed view of the mesh is provided in Fig. 3.

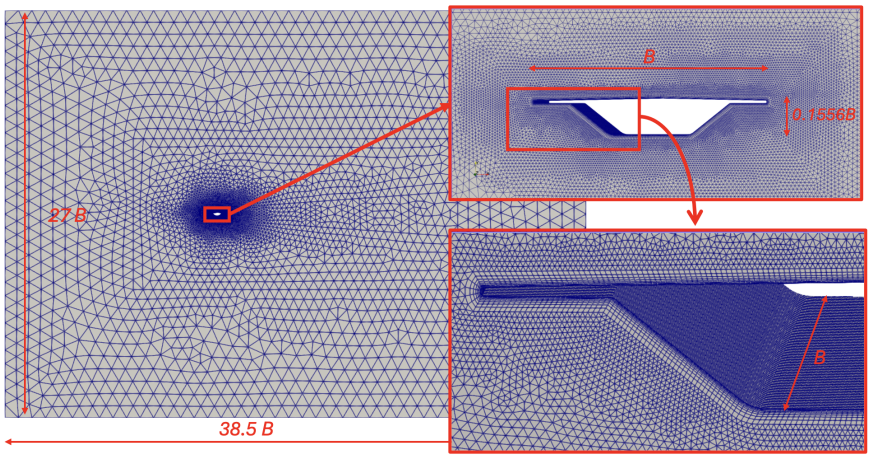

Fig. 3. Details of the spatial discretization of the 3D computational domain.

Table 1. Distribution of mesh cells. Maximum and minimum cell sizes and growth rates in different refinement regions of the computational domain. The number of cells refers to a two-dimensional $x - y$ plain.

Region	Min. Size [m]	Max. Size [m]	Growth Rate	# of cells (2D)
A	0.012	0.02	0.01475	24,816
B	0.030	0.04	0.02750	2,469
C	0.040	0.12	0.05625	1,686
D	0.100	0.20	0.09000	8,300
E	0.140	0.20	0.20000	9,417

3.3 Boundary conditions

The boundary conditions for the simulation are defined as follows. At the domain inlet, a uniform velocity ($U = 20\,\mathrm{m\,s}$) in the positive x-direction is specified using a Dirichlet condition, while a Neumann condition is applied for pressure. At the outlet, a Dirichlet boundary condition is specified for pressure ($P = 0$), while the normal gradient of velocity is specified to be zero. The top and bottom boundaries of the computational domain are treated as slip walls, characterized by zero normal velocity and zero normal gradients for both tangential velocity components and pressure. Finally, the surface of the bridge deck is modeled as a no-slip wall, enforcing zero fluid velocity relative to the structure.

3.4 Validation and verification studies

The quality of the simulation was assessed by conducting verification and validation studies. Table 2 reports the sensitivity of the simulation to the spatial discretization in terms of force coefficients. Three meshes were compared, including $\sim$4.3 M, $\sim$7.7 M, and $\sim$14.8 M elements. In general, results show negligible variations for the C_D and C_M values, and acceptable performance for C_L. Similarly, the temporal discretization sensitivity is reported in Table 3, showing again acceptable values.

Table 2. Spatial discretization study comparing the time-averaged force coefficients using three different meshes.

Mesh	No. of cells	C_D	C_L	C_M
Coarse	4,354,800	0.0758	-0.1267	0.1069
Medium	7,790,700	0.0733	-0.1049	0.1070
Fine	14,855,200	0.0672	-0.0865	0.1075

Table 3. Time discretization study comparing the time-averaged forced coefficient using three different Courant numbers.

Co	dt	C_D	C_L	C_M
2.0	$1.874 \cdot 10^{-04}$	0.0764	-0.1421	0.1035
1.0	$9.580 \cdot 10^{-05}$	0.0733	-0.1049	0.1070
0.5	$5.123 \cdot 10^{-05}$	0.0696	-0.0829	0.1080

Results are also compared with other studies available in the literature for the same cross-section geometry, including wind tunnel tests and CFD simulations,

as reported in Table 4. While there is a reasonable agreement for C_D and C_M across the board, some variations are found in the reported values for the C_L, which may be caused by the sensitivity of the result to the roundness of the bottom corner, as discussed in [10].

Table 4. Validation study comparing the time-averaged force coefficients with relevant publications found in the literature.

Reference	Method	C_D	C_L	C_M
Mannini et al. (2016) [18]	Experimental	0.107	-0.191	0.101
Mannini et al. (2010) [18]	2D URANS LEA	0.067	-0.027	0.102
Fransos and Bruno (2010) [10]	2D URANS $k-\omega$ SST	0.076	-0.096	-
Verma et al. (2024) [30]	2D URANS $k-\omega$ SST	0.068	-0.120	0.095
Current study	3D LES	0.073	-0.105	0.107

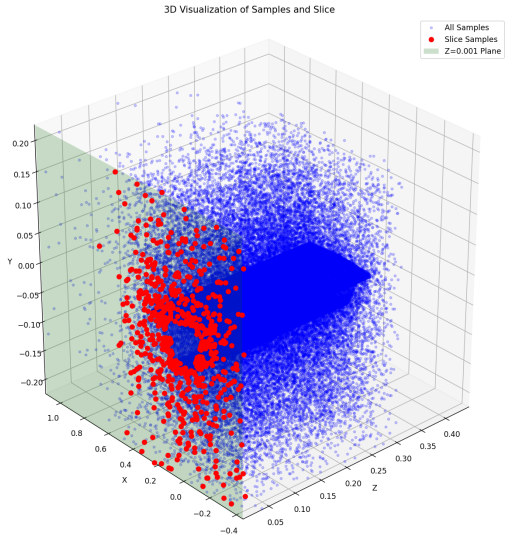

Fig. 4. Importance sampling in the 3D flow domain guided by the Signed Distance Function (SDF) to increase the accuracy around the bridge deck using a resolution of $150 \times 96 \times 32$.

4 Preliminary Results

4.1 Flow domain sampling

Fig. 4 shows the set of samples obtained using the proposed 3D importance sampling strategy based on the SDF concept described in Section 2.1. To facilitate its interpretation, a plane at Z=0.001 with all its samples ($150 \times 96 \times 32$) is marked in the representation, where it can be seen that the number of samples grows as we get closer to the bluff body surface, following the priorities dictated by the SDF. Such adaptive sampling is pivotal for accurately extracting relevant flow features in the neighborhood of the deck surface, an essential step for the precise estimation of wind-induced forces.

4.2 Flow field representation using 3D image volumes

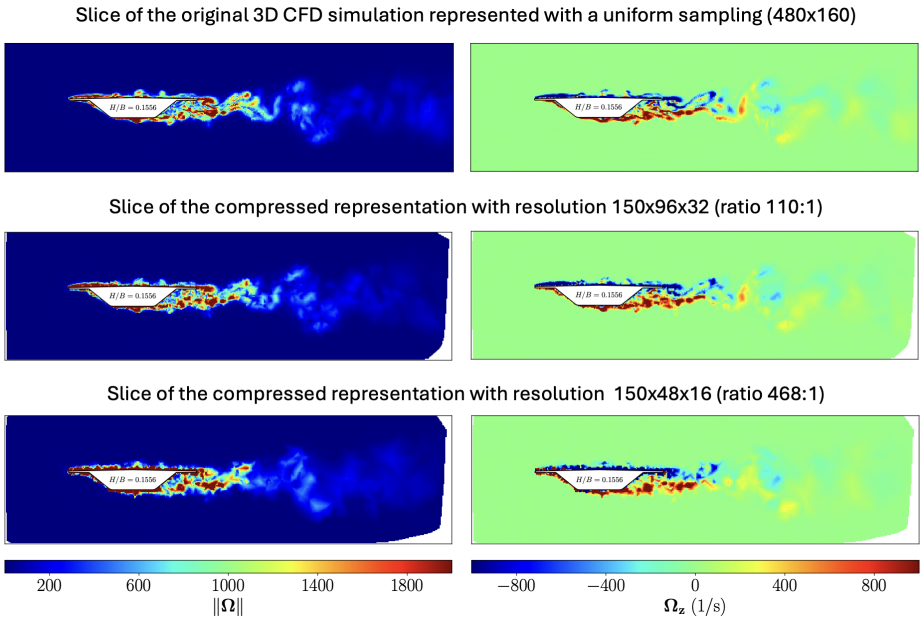

Fig. 5. Instantaneous vorticity ($\boldsymbol{\Omega}$) flow fields at time step $t = 1.000048072$ s obtained from a slice of the original CFD simulation represented using a uniform sampling strategy with a resolution of 480×160. The flow field 3D images are sampled with resolutions of $150 \times 96 \times 32$ and $150 \times 48 \times 16$, leading to compression ratios of 110:1 and 468:1, respectively.

Fig. 5 presents a comparison of time-dependent vorticity fields at time step $t = 1.000048072$ s on an $X-Y$ plane slice, oriented perpendicular to the spanwise

axis of the flow domain. The figure compares the original 3D CFD simulation, visualized on this slice via an image obtained using uniform sampling and linear interpolation at a resolution of 480×160, with fields reconstructed from two compressed representations of the 3D volume, corresponding to effective resolutions of (1) $150 \times 96 \times 32$ and (2) $150 \times 48 \times 16$ voxels. The comparison reveals that the compressed volumes yield a high-fidelity representation of the flow field in the vicinity of the bridge deck, while exhibiting progressively reduced accuracy in far-field regions, notably in the distant wake. This results align with the design objectives of our sampling strategy, which prioritizes accuracy in regions critical for the extraction and subsequent emulation of wind-induced forces. This trade-off between far-field accuracy and data size becomes more pronounced at lower effective resolutions, resulting in higher compression ratios.

Fig. 6 illustrates the three-dimensional pressure distribution across the deck surface, comparing the original CFD simulation results with those reconstructed from a compressed representation having an effective resolution of $150 \times 48 \times 16$ voxels. Accurate reproduction of the pressure distribution is critical for the precise assessment of wind-induced loads on the bridge deck. The figure demonstrates that the proposed sampling strategy effectively captures instantaneous pressure features, such as those observable in the bottom windward (left) corner of the visualized deck, indicating that the sampling strategy accurately preserves the spanwise characteristics of the flow, while achieving a compression ratio of 468:1. This ratio can be further augmented by integrating an additional INR compression layer, as detailed in Section 2.2. Preliminary results incorporating this subsequent layer demonstrate compression ratios reaching 3000:1, with a corresponding Mean Average Precision Error (MAPE) of 7.2 % for the reconstructed fields.

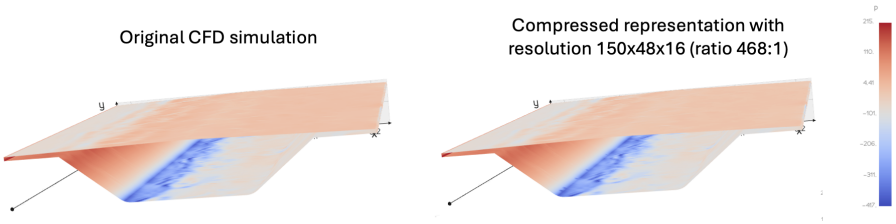

Fig. 6. Instantaneous pressure ($\boldsymbol{p}$) distribution along the deck surface at time step $t = 1.000048072$ s obtained from the original CFD simulation and the flow field image volume with a resolution of $150 \times 48 \times 16$, leading to a compression ratio of 468:1.

5 Concluding remarks and ongoing research

Our sampling strategy achieves substantial compression ratios, typically in the 10^3-10^4 range, while ensuring high-fidelity reproduction of critical flow field char-

acteristics around an immersed bluff body. Future research will concentrate on improving performance by designing an improved decoding stage with a more efficient architecture for processing volumetric data, with the objective of attaining even greater overall compression ratios. This ability to efficiently manage and analyze massive flow fields has remarkable benefits in modern engineering applications. The developed scheme allows researchers to tackle problems that otherwise would be impossible due to data size limitations, such as large dataset storage and computational applications involving iterative processes, such as AI training, optimization, uncertainty quantification, reliability analyses, or reliability-based design optimization. Future investigations will integrate this methodology into deep learning emulation frameworks for efficient and accurate wind-resistant design of wind-sensitive structures.

Acknowledgements Investigation funded by the NSF (Grant No. CMMI-2503131). Omar A. Mures acknowledges partial support by Xunta de Galicia (Refs. ED431C 2021/30 & ED431G 2023/01), and the Galician Supercomputing Center (CESGA), funded by the European Regional Development Fund (ERDF), the Spanish Ministry of Science and Innovation, and the Galician Government. Miguel Cid Montoya thanks the start-up funds by Clemson University.

Bibliography

[1] Ainsworth, M., Tugluk, O., Whitney, B., Klasky, S.: Multilevel techniques for compression and reduction of scientific datathe univariate case. Computing and Visualization in Science **19**(5), 65–76 (2018)

[2] Alvarez, A., Nieto, F.: Vortex induced vibration analysis of a twin-box bridge deck by means of 3d les simulationss. J Wing Eng Ind Aerod **258**, 106015 (2025)

[3] Bergman, K., Borkar, S., Campbell, D., Carlson, W., Dally, W., Denneau, M., Franzon, P., Harrod, W., Hill, K., Hiller, J.: Exascale computing study: Technology challenges in achieving exascale systems. Defense Advanced Research Projects Agency Information Processing Techniques Office (DARPA IPTO), Tech. Rep **15**, 181 (2008)

[4] Blocken, B.: 50 years of computational wind engineering: Past, present and future. J. Wind Eng. Ind. Aerod. **129**, 69–102 (2014)

[5] Cid Montoya, M.: Sequential aero-structural optimization method for efficient bridge design. Comput-Aided Civ Inf **39**(3), 319–344 (2024)

[6] Cid Montoya, M., Mishra, A., Verma, S., Mures, O.A., Rubio-Medrano: Aeroelastic force prediction via temporal fusion transformers. Comput-Aided Civ Inf pp. 1–32 (2024)

[7] Cleary, J., Witten, I.: Data compression using adaptive coding and partial string matching. IEEE transactions on Communications **32**(4), 396–402 (1984)

[8] Deutsch, P.: Rfc1951: Deflate compressed data format specification version 1.3 (1996)

[9] van Druenen, T., Blocken, B.: Cfd simulations of cyclist aerodynamics: Impact of computational parameters. J Wind Eng Ind Aerodyn **249**, 105714 (2024)

[10] Fransos, D., Bruno, L.: Edge degree-of-sharpness and free-stream turbulence scale effects on the aerodynamics of a bridge deck. J Wing Eng Ind Aerod **98**, 661–671 (2010)

[11] Fu, R., Paden, I., Garcia-Sanchez, C.: Should we care about the level of detail in trees when running urban microscale simulations? Sustainable Cities and Society **101**, 105143 (2024)

[12] Gao, H., Hu, G., Zhang, D., Jiang, W., Tse, K.T., Kwok, K.C.S., Kareem, A.: Urban wind field prediction based on sparse sensors and physics-informed graph-assisted auto-encoder. Computer-aided Civil and Infrastructure Engineering **39**, 1409–1430 (2024)

[13] Kilmer, M.E., Horesh, L., Avron, H., Newman, E.: Tensor-tensor algebra for optimal representation and compression of multiway data. PNAS **118**(28), e2015851118 (2021)

[14] Li, Z., Wang, M., Pi, H., Xu, K., Mei, J., Liu, Y.: E-nerv: Expedite neural video representation with disentangled spatial-temporal context. In: European Conference on Computer Vision. pp. 267–284. Springer (2022)

[15] Lu, Y., Jiang, K., Levine, J.A., Berger, M.: Compressive neural representations of volumetric scalar fields. Computer Graphics Forum **40**(3), 135–146 (2021)

[16] Luo, X., Lurvey, S., Huang, Y., Ren, Y., Huang, J., Yoon, B.J.: Efficient compression of sparse accelerator data using implicit neural representations and importance sampling. arXiv preprint arXiv:2412.01754 (2024)

[17] Mannini, C., Sbragi, G., Schewe, G.: Analysis of self-excited forces for a box-girder bridge deck through unsteady rans simulations. Journal of Fluids and Structures **63**, 57–76 (2016)

[18] Mannini, C., oda, A., VoSS, R., Schewe, G.: Unsteady RANS simulations of flow around a bridge section. J Wing Eng Ind Aerod **98**, 742–753 (2010)

[19] Melaku, A.F., Bitsuamlak, G.T.: Prospect of les for predicting wind loads and responses of tall buildings: A validation study. J Wind Eng Ind Aerodyn **244**, 105613 (2024)

[20] Nicoud, F., Ducros, F.: Subgrid-scale stress modelling based on the square of the velocity gradient tensor. Flow Turbulence and Combustion **62**(3), 183200 (1999)

[21] Osher, S., Fedkiw, R.: Constructing signed distance functions. Level set methods and dynamic implicit surfaces pp. 63–74 (2003)

[22] Pan, S., Brunton, S.L., Kutz, J.N.: Neural implicit flow: a mesh-agnostic dimensionality reduction paradigm of spatio-temporal data. Journal of Machine Learning Research **24**(41), 1–60 (2023)

[23] Patruno, L.: Accuracy of numerically evaluated flutter derivatives of bridge deck sections using RANS: Effects on the flutter onset velocity. Eng. Struct. **89**, 4965 (2015)

[24] Popescu, M.C., Balas, V.E., Perescu-Popescu, L., Mastorakis, N.: Multilayer perceptron and neural networks. WSEAS Transactions on Circuits and Systems **8**(7), 579–588 (2009)

[25] Sarwar, M.W., Ishihara, T., Shimada, K., Yamasaki, Y., Ikeda, T.: Prediction of aerodynamic characcteristics of a box girder bridge section using LES turbulence model. J Wing Eng Ind Aerod **96**, 1895–1911 (2008)

[26] Schindler, M.: A fast block-sorting algorithm for lossless data compression. In: Proc. Data Compression Conf. vol. 469. Citeseer (1997)

[27] Shannon, C.E.: A mathematical theory of communication. The Bell system technical journal **27**(3), 379–423 (1948)

[28] Tancik, M., Srinivasan, P., Mildenhall, B., Fridovich-Keil, S., Raghavan, N., Singhal, U., Ramamoorthi, R., Barron, J., Ng, R.: Fourier features let networks learn high frequency functions in low dimensional domains. Advances in neural information processing systems **33**, 7537–7547 (2020)

[29] Vaswani, A., Shazeer, N., Parmar, N., Uszkoreit, J., Jones, L., Gomez, A.N., Kaiser, Ł., Polosukhin, I.: Attention is all you need. Advances in neural information processing systems **30** (2017)

[30] Verma, S., Cid Montoya, M., Mishra, A.: Shape- and frequency-dependent self-excited forces emulation for the aero-structural design of bluff deck bridges. J. Wind Eng. Ind. Aerod. **252**, 105769 (2024)

[31] Zhang, J., Wang, W., Wang, C., Hua, X., Huang, Z.: Numerical investigation on vertical vortex-induced vibrations of triple-box girders with curved and linear-type webs. J Wing Eng Ind Aerod **242**, 105589 (2023)
[32] Ziv, J., Lempel, A.: Compression of individual sequences via variable-rate coding. IEEE transactions on Information Theory **24**(5), 530–536 (1978)